

# Dynamical screening in $\text{La}_2\text{CuO}_4$

Philipp Werner,<sup>1</sup> Rei Sakuma,<sup>2</sup> Fredrik Nilsson,<sup>2</sup> and Ferdi Aryasetiawan<sup>2</sup>

<sup>1</sup>*Department of Physics, University of Fribourg, 1700 Fribourg, Switzerland*

<sup>2</sup>*Department of Physics, Division of Mathematical Physics,  
Lund University, Sölvegatan 14A, 223 62 Lund, Sweden*

(Dated: September 9, 2018)

We show that the dynamical screening of the Coulomb interaction among Cu- $d$  electrons in high- $T_c$  cuprates is very strong and that a proper treatment of this effect is essential for a consistent description of the electronic structure. In particular, we find that ab-initio calculations for undoped  $\text{La}_2\text{CuO}_4$  yield an insulator only if the frequency dependence of the Coulomb interaction is taken into account. We also identify a collective excitation in the screened interaction at 9 eV which is rather localized on the copper site, and which is responsible for a satellite structure at energy  $-13$  eV, located below the  $p$  bands.

PACS numbers: 71.20.-b, 71.27.+a

## I. INTRODUCTION

The discovery of superconductivity with high transition temperature  $T_c$  in iron pnictide compounds<sup>1</sup> has triggered a reexamination of the basic theoretical assumptions about the electronic structure of the copper oxide superconductors,<sup>2,3</sup> based on the similarities and differences between the two classes of materials. The role and strength of electronic correlations in high-temperature superconductors is a much debated, but still not completely settled issue. One of the fundamental problems in the theoretical description of a correlated material is the downfolding of the full many-electron Hamiltonian into a low-energy model with a few orbitals believed to be most relevant for the origin of superconductivity. In the case of the cuprates, it is generally agreed that the most relevant orbitals are those that span the two-dimensional copper oxide layers, namely, Cu  $d_{x^2-y^2}$  and O  $p_x$  and  $p_y$  orbitals, although models that include the apical O  $p_z$  as well as Cu  $d_{z^2}$  orbitals have also been considered.<sup>4</sup> Two prominent low-energy models are the one-band model consisting of only the strongly hybridized anti-bonding combination of Cu  $d_{x^2-y^2}$  and O  $p_x$  and  $p_y$  orbitals and a three-band model which also includes the bonding combination of  $d_{x^2-y^2}$  and  $p_{x,y}$  and the non-bonding  $p$  orbital, also known as the Emery model.<sup>5</sup> Since the stoichiometric compounds are usually classified as charge-transfer insulators, a proper description of the low-energy properties should involve the Cu  $d_{x^2-y^2}$  and two oxygen  $p_\sigma$  orbitals.

A physically well-motivated representation of the underlying one-particle band structure of these models can be constructed by a tight-binding fit to the *ab-initio* band structure calculated from the local density approximation (LDA). Since the Coulomb interaction among the  $d$  electrons is so large that a nonperturbative treatment of the correlation effects is needed, an interaction term is then added on top of the one-particle Hamiltonian leading to the Hubbard model with an effective interaction  $U$ . The material-specific determination of the Hubbard  $U$  is, however, a subtle and complicated task. It

can be shown that a reduction of the Hamiltonian to a low-energy model necessitates the introduction of a frequency-dependent  $U$  reflecting the retarded electron-electron interaction resulting from the elimination of the high-energy portion of the original Hamiltonian. In other words, the frequency-dependent  $U$  incorporates the effects of the high-energy component of the Hamiltonian which has been projected out in the low-energy model.

A large body of theoretical studies on the cuprates can be found in the literature. Several recent works employed a combination of density functional calculations in the local density approximation and dynamical mean field theory (LDA+DMFT) in order to investigate one-band and three-band models of undoped cuprates. The issues discussed in these works are the importance of antiferromagnetism in opening a gap, or its effect on the gap size,<sup>6</sup> the proper choice of the  $d$ - $p$  level splitting<sup>7</sup> and the difference of the electronic structure of  $\text{La}_2\text{CuO}_4$  in the T and T' crystal structures.<sup>8</sup> It was also shown that the interatomic interaction between  $p$  and  $d$  electrons plays an important role in stabilizing the charge-transfer insulator state, and therefore needs to be considered at least at the Hartree level.<sup>9</sup> While some of these studies used realistic bandstructures, the interaction parameters were chosen in an ad-hoc fashion and as far as we know, all low-energy models for the cuprates considered so far have neglected the effects of the frequency dependence of  $U$ .

The calculation of the Coulomb matrix elements in a Wannier basis corresponding to the low-energy subspace (here the one-band or three-band model) is possible using the constrained random phase approximation (cRPA).<sup>11</sup> This formalism yields interaction parameters which vary from a static value of a few eV (significantly smaller than the values typically adopted in previous studies) to bare interactions of the order of 20 eV at high frequency. The importance of properly treating this frequency dependence has been pointed out in previous papers,<sup>12-15</sup> but not for the cuprates. As we will show, the screening effect in high- $T_c$  cuprates is remarkably strong. There are even recent experimental studies which suggest a connection between screening and  $T_c$ .<sup>16</sup>

Four issues will be addressed in the present work: First, what is the role of the frequency-dependent  $U$ ? Second, is a one-band model sufficient to describe the low-energy electronic structure of the undoped cuprates? Third, what is the role of the interaction between the Cu  $d$  and O  $p$  electrons that is usually neglected in most studies? Fourth, do *ab-initio* calculations support the conventional classification of undoped cuprates as charge-transfer insulators? The third issue has recently been considered in a model study based on adjustable, static interaction parameters.<sup>9</sup> Here, we focus on the prototypical high- $T_c$  material  $\text{La}_2\text{CuO}_4$  which has been thoroughly investigated both experimentally and theoretically.<sup>10</sup> Our strategy is to perform a “true” *ab-initio* simulation of the electronic structure of  $\text{La}_2\text{CuO}_4$ , as accurately as possible with current technology, and to check if it gives a faithful representation of the low-energy electronic properties. To take into account electron correlations, we use the DMFT method and solve the impurity problem with dynamic  $U$  using a continuous-time quantum Monte Carlo (CT-QMC) algorithm. In addition to the *ab-initio* bandstructure we also use the corresponding *ab-initio* interaction parameters  $U$  obtained from the cRPA method. We find that *ab-initio* calculations which neglect the frequency dependence of this interaction fail to produce an insulating solution. On the other hand, if the frequency dependence of the  $d$ - $d$  interaction is taken into account, a three-band simulation based on *ab-initio* interaction parameters produces an insulator with a gap size in good agreement with experiment.

The paper is organized as follows. Section II discusses the methods used to derive the low-energy models (one-band and three-band) and the LDA+DMFT approach used to solve these models. Section III shows the spectral functions obtained for  $\text{La}_2\text{CuO}_4$  using either the static values of the estimated Coulomb interactions, or the frequency dependent  $d$ - $d$  interaction. Section IV is a summary and conclusion.

## II. MODEL AND METHOD

### A. LDA bandstructure

Figure 1 shows the LDA bandstructure as well as the bandstructures of the effective low energy one- and three-band models. The LDA bandstructure was computed with the full-potential linearized augmented-plane-wave (FLAPW) code FLEUR<sup>17</sup> and the model subspaces were defined using symmetry constrained maximally localized Wannier functions as implemented in the WANNIER90 library.<sup>18–22</sup> The effective one-band model consists of a single orbital of  $d_{x^2-y^2}$  character at each Cu site. For the three-band model we increase the model subspace to include also the two in-plane Wannier orbitals of O  $p_x/p_y$  character. It should be noted that, although the conduction bands look very similar in the two cases the Wannier functions corresponding to the Cu  $d_{x^2-y^2}$  orbitals

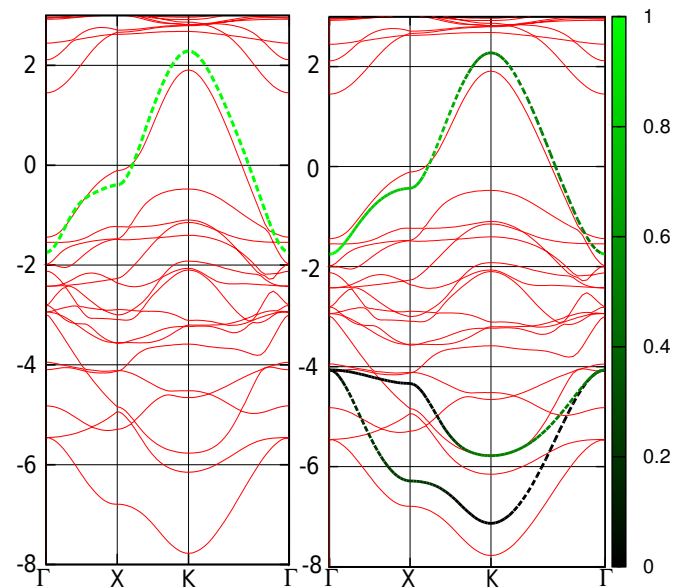


FIG. 1: LDA bandstructure (solid lines). In addition the left panel shows the Wannier interpolated band structure for the one-band model and the right panel the corresponding band structure for the three-band model (thick dashed lines). The color coding in the right panel indicates the  $d$ -character of the bands. The symmetry points are defined as  $\Gamma = (0, 0)$ ,  $K = (\pi, \pi)$  and  $X = (\pi, 0)$ .

are very different. In the one-band case the Cu-centred Wannier function is constructed as a linear combination of only a few bands close to the Fermi energy. This leads to less variational freedom and hence much more delocalized Wannier functions than in the three-band case, where more states are used to construct the Wannier functions. Hence, while in the one-band case there is a one to one correspondence between the conduction band and the  $d_{x^2-y^2}$ -like Wannier function spanning the correlated subspace, this is not the case for the three-band model. In the three-band model the conduction band can be interpreted as the antibonding combination of the  $p$  and  $d$  states and the two valence bands can be interpreted as the bonding and nonbonding combinations. Therefore, although the main  $d$ -weight is in the conduction band, there is also a small  $d$ -weight in the valence bands as can be seen in the right panel of Fig. 1.

### B. cRPA calculation

We compute the frequency-dependent interaction parameters for the one-band and three-band model using cRPA.<sup>11</sup> In this scheme, the polarization function  $P(\omega)$  is calculated in the random phase approximation, i.e. by considering only the bubble diagrams with LDA propagators. This polarization function relates the bare interaction  $V$  and the fully screened Coulomb interaction  $W(\omega)$  via

$$W(\omega) = V + VP(\omega)W(\omega).$$

One then defines a polarization  $P_l(\omega)$  associated with transitions between states defined in the low-energy bands. Since these transitions will be treated explicitly in the DMFT calculation, we remove these screening processes in the calculation of the effective interaction. For this, one computes  $P_r(\omega) = P(\omega) - P_l(\omega)$  and the frequency-dependent  $U(\omega)$  which satisfies

$$W(\omega) = U(\omega) + U(\omega)P_l(\omega)W(\omega).$$

Apparently, the screening of  $U(\omega)$  by  $P_l(\omega)$  gives the fully screened interaction  $W(\omega)$ . One thus interprets  $U(\omega)$  as an effective frequency-dependent interaction among electrons residing in the low energy subspace defining the Hilbert space of the low-energy model. This so-called Hubbard  $U$  can also be obtained by solving the following equation:

$$U(\mathbf{r}, \mathbf{r}'; \omega) = V(\mathbf{r}, \mathbf{r}') + \int d^3r_1 d^3r_2 V(\mathbf{r}, \mathbf{r}_1) P_r(\mathbf{r}_1, \mathbf{r}_2; \omega) U(\mathbf{r}_2, \mathbf{r}'; \omega), \quad (1)$$

or schematically  $U(\omega) = [1 - VP_r(\omega)]^{-1}V$ . The frequency-dependent interaction parameters of the model are then given by the matrix elements of  $U(\omega)$  in the Wannier basis  $\{\varphi_m\}$  constructed using the procedure of Marzari and Vanderbilt.<sup>18</sup>

$$\langle \varphi_{m_1} \varphi_{m_2} | U(\omega) | \varphi_{m_3} \varphi_{m_4} \rangle = \int d^3r d^3r' \varphi_{m_1}^*(\mathbf{r}) \varphi_{m_2}(\mathbf{r}) \times U(\mathbf{r}, \mathbf{r}'; \omega) \varphi_{m_3}(\mathbf{r}') \varphi_{m_4}^*(\mathbf{r}'). \quad (2)$$

While the application of this procedure to the one-band model is unambiguous, the three-band case is more subtle. Here, the subset of screening processes which should be excluded depends on how the three-band model is solved. If we were to solve the full three-band model, we would simply remove all screening processes within the model and no ambiguity would arise. It would, however, lead to a multi-site impurity problem involving not only the copper site but also the oxygen sites and orbital-dependent  $U(\omega)$ . At present it is not possible to perform DMFT calculations for such a complex problem. In this work, we will treat the  $d$ - $d$  interactions within DMFT, and the  $p$ - $p$  and  $p$ - $d$  interactions at the Hartree level (similar to Ref. 9). In this case, only the  $d$ - $d$  screening needs to be removed in the calculation of  $U$  since we do not include  $p$ - $d$  screening processes in the model. According to the discussion in the previous section, the main  $d$ -weight is in the conduction band. We therefore remove only the screening within the conduction band also for the three-band model. The effective interaction  $U(\mathbf{r}, \mathbf{r}'; \omega)$  as defined in Eq. (1) is then the same as in the one-band model but the matrix elements of  $U$  as defined in

Eq. (2) representing the interaction between  $d$ -electrons will nevertheless be different from the one-band case, because the Wannier orbitals of the three-band model are significantly more localized.

### C. DMFT calculation

The LDA calculation and cRPA downfolding lead to a low energy effective model with one or three bands and dynamically screened (retarded) intra- and inter-orbital interactions. To solve this model, we use the DMFT method.<sup>23</sup> This approximation maps the lattice problem onto a single-orbital Anderson impurity model with a dynamical interaction  $U_{dd}(\omega)$ , i.e. an electron-boson problem with a Holstein-like coupling to a continuum of bosonic modes.<sup>12</sup> Using the hybridization-expansion Monte Carlo method,<sup>24,25</sup> this impurity problem can be solved efficiently and without approximations on the imaginary axis, yielding the impurity Green's function  $G_{\text{imp}}(i\omega_n)$  and the impurity self-energy  $\Sigma_{\text{imp}}(i\omega_n)$ .

In the one-band model, we approximate the lattice self-energy  $\Sigma(k, i\omega_n)$  by  $\Sigma_{\text{imp}}(i\omega_n)$  and compute the local lattice Green's function as

$$G_{\text{loc}}(i\omega_n) = \int (dk) [i\omega_n + \mu - \varepsilon_k - \Sigma_{\text{imp}}(i\omega_n)]^{-1}.$$

Here, the  $k$ -integral is normalized over the Brillouin zone, and  $\varepsilon_k$  is the conduction band dispersion. The chemical potential  $\mu$  is adjusted to ensure one  $d$ -electron per unit cell, so we do not need a “double counting term” to remove the Hartree-type self-energy contribution which is already included at the LDA level.

The three-band case needs some justification. Let us start with the Hamiltonian with a static  $U = U(\omega = 0)$  given by

$$H = H_0 + U_{dd} \sum_i n_{id\uparrow} n_{id\downarrow} + U_{pp} \sum_j n_{jp\uparrow} n_{jp\downarrow} + U_{pd} \sum_{\langle ij \rangle} n_{id} n_{jp}, \quad (3)$$

where  $n = n_{\uparrow} + n_{\downarrow}$ ,  $H_0$  is the tight-binding Hamiltonian for the three-band model and  $i$  and  $j$  label the copper and oxygen sites, respectively. Since the  $p$  bands are filled, correlation effects among  $p$  electrons are expected to be small and the LDA bands should be quite reliable. The impurity problem is therefore solved only for the copper site and since we do not consider  $p$  to  $d$  screening channels in the model, the effective interaction  $U_{dd}$  must include these  $p$ - $d$  screening processes and therefore corresponds to the one-band model, albeit evaluated with the more localized Wannier functions of the three-band model, as discussed earlier. We now take into account the frequency dependence of  $U_{dd}$  and solve the impurity problem with a dynamic  $U_{dd}$  using the CT-QMC method within the

action formalism. In the three-band case, we consider, in addition to the local self-energy  $\Sigma_{dd}(i\omega_n) = \Sigma_{\text{imp}}(i\omega_n)$  the  $p$ - $p$  and  $p$ - $d$  interactions at the Hartree level. We thus have to add double counting terms  $\Sigma_{DC}$ , which as in Ref. 9 we evaluate with the LDA densities for the  $U_{pp}$  and  $U_{pd}$  contributions. This amounts to adjusting the Hartree self-energies (which are included in the LDA) to the self-consistently computed densities. For  $\Sigma_{dd}$ , we use a standard double-counting term<sup>26</sup> evaluated with the correlated density  $n_d$ .<sup>27</sup> Specifically, the diagonal matrix elements of  $\tilde{\Sigma} = \Sigma - \Sigma_{DC}$  are

$$\tilde{\Sigma}_{dd}(i\omega_n) = \Sigma_{\text{imp}}(i\omega_n) - U_{dd}(0)(n_d - \frac{1}{2}) + 4U_{pd}(0)(n_p - n_p^{LDA}), \quad (4)$$

$$\tilde{\Sigma}_{pp}(i\omega_n) = U_{pp}(0)(n_p - n_p^{LDA}) + 2U_{pd}(0)(n_d - n_d^{LDA}), \quad (5)$$

and the off-diagonal elements are set to zero. The factor of four in the last term of  $\tilde{\Sigma}_{dd}$  is due to the presence of four nearest oxygen atoms around a copper atom and the factor of two in the last term of  $\tilde{\Sigma}_{pp}$  is due to the presence of two nearest copper atoms around an oxygen atom. Note that in the Hartree-like terms, we use the screened interactions. While this can be justified in the case of the  $d$ - $d$  interaction,<sup>13</sup> it is an approximation for the  $U_{pp}$  and  $U_{pd}$  terms which should be considered as a lower bound estimate. At present, it is unclear how the frequency-dependence should be incorporated into a static description if the screening modes for different interaction terms are different.

With this approximate self-energy, we then compute the local lattice Green's function as

$$G_{\text{loc}}(i\omega_n) = \int (dk) [(i\omega_n + \mu)\mathcal{I} - H_k - \tilde{\Sigma}(i\omega_n)]^{-1}$$

which is a  $3 \times 3$  matrix, and then extract the  $d$ -component in order to define a new hybridization function for the impurity model. In the self-consistent iteration, the chemical potential is adjusted such that the total number of  $p$ - and  $d$ -electrons is  $\sum_{\alpha=1}^3 G_{\alpha\alpha}(\tau = 0_-) = 5$ .

#### D. Analytical continuation

In order to compute spectral functions for models with frequency dependent interactions, one can use the strategy proposed in Ref. 29. We define the bosonic function  $\exp[-K(\tau)]$ , with

$$K(\tau) = \frac{1}{\pi} \int_0^\infty d\omega' \frac{\text{Im}U(\omega')}{\omega'^2} [b(\omega', \tau) - b(\omega', 0)]$$

and  $b(\omega', \tau) = \cosh[(\tau - \beta/2)\omega'] / \sinh[\beta\omega'/2]$ , and compute the auxiliary Green's function  $G_{\text{aux}}(\tau) = G_{dd}(\tau) / \exp[-K(\tau)]$ . The spectral function corresponding to  $G_{\text{aux}}(\tau)$  is expected to have no high-frequency

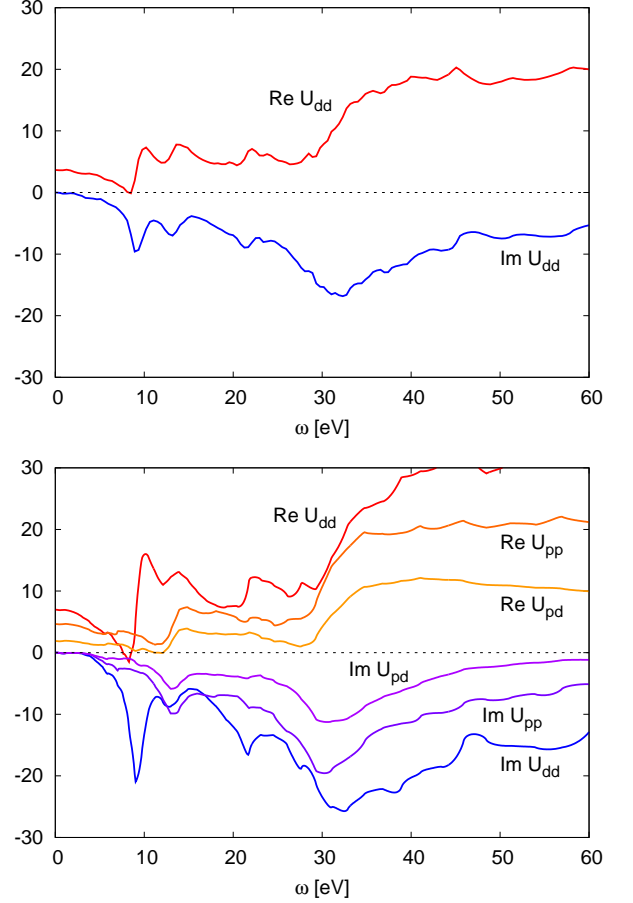


FIG. 2: Dynamically screened interactions in the one-band model (top panel) and in the three-band model (bottom panel). Because only the  $d$ -orbital is considered in the impurity calculation, we only remove the  $d$ - $d$  screening in the three-orbital case.

components and can be obtained using the maximum entropy analytical continuation procedure.<sup>30</sup> Finally, the spectral function  $A$  for  $G$  is obtained from a convolution of the auxiliary spectral function  $A_{\text{aux}}$  and the exactly computable spectral function of the bosonic factor  $\exp[-K(\tau)]$ .<sup>13,29</sup> In this convolution, the low-energy structures of the spectral function are replicated at energies which are directly related to the dominant screening modes.

We can employ the same strategy to analytically continue the self-energy. For this, we first compute a Green's function  $\tilde{G}(i\omega_n) = 1/(i\omega_n + \tilde{\mu} - \Sigma(i\omega_n))$  with a suitably chosen  $\tilde{\mu}$  and apply the above procedure to obtain the corresponding spectral function  $\tilde{A}(\omega)$  and (using the Kramers-Kronig transformation) the Green's function  $\tilde{G}(\omega)$ . The real-frequency self-energy, including high-energy features, is then given by  $\Sigma(\omega) = \omega + \tilde{\mu} - 1/\tilde{G}(\omega)$ .

### III. RESULTS

#### A. Frequency-dependent $U$

We plot the cRPA results for  $\text{La}_2\text{CuO}_4$  in Fig. 2. The top panel shows  $U_{dd}(\omega)$  for the one-band model and the bottom panel shows  $U_{dd}(\omega)$ ,  $U_{pp}(\omega)$  and  $U_{pd}(\omega)$  for the three-band model. In the one-band case, the static (screened) interaction is  $U_{dd}(\omega = 0) = 3.65$  eV. The imaginary part of  $U$ , which describes the excitation spectrum of the system excluding contributions from the model, is characterized by several collective excitations: a broad peak centered at  $\omega = 30$  eV and a sharp peak at  $\omega = 9$  eV, as well as smaller peaks around  $\omega = 13$  and 21 eV. The broad peak corresponds to a collective plasmon excitation that is coupled to single-particle excitations providing decaying channels responsible for the broad feature. The pole-like structure around  $\omega = 9$  eV may be interpreted as a collective subplasmon excitation arising from single-particle transitions from the occupied oxygen  $p$  bands to the unoccupied part of the anti-bonding  $d_{x^2-y^2}$  band. At very high-energy above the plasmon frequency, screening becomes ineffective and the interaction approaches the bare Coulomb interaction value of  $U_{dd} \approx 20$  eV.

In the three-band case, the structures of the frequency-dependent  $U_{dd}$  interaction look similar to the one-band case but the static value is  $U_{dd}(\omega = 0) = 7.00$  eV, while the high frequency limit is about 30 eV. These higher values result from the more localized Wannier orbitals because, as explained previously,  $U_{dd}$  is calculated as a matrix element of the  $U(\mathbf{r}, \mathbf{r}'; \omega)$  of the one-band model. The static values of the  $p$ - $p$  and  $p$ - $d$  interactions are  $U_{pp}(\omega = 0) = 4.64$  eV and  $U_{pd}(\omega = 0) = 1.88$ . For these interactions, the dominant low-frequency pole is near 13 eV (the peak at 9 eV is missing). Since  $U_{dd}$ ,  $U_{pp}$ , and  $U_{pd}$  are calculated as matrix elements of the *same*  $U(\mathbf{r}, \mathbf{r}'; \omega)$ , the presence of a strong peak in  $\text{Im } U_{dd}$  but not in  $\text{Im } U_{pp}$  and  $\text{Im } U_{pd}$  implies that the collective excitation corresponding to the 9 eV peak is not extended, as in usual plasmon-like excitations, but rather localized on the copper site. This suggests that the screening mechanism of a hole or a test charge created at the copper site will be rather different from the screening mechanism at the oxygen sites. An additional screening charge fluctuation associated with the 9 eV peak is present in response to a hole created at the copper site but not at the oxygen sites. For  $\text{HgBa}_2\text{CuO}_4$ , another high- $T_c$  cuprate compound, one can identify the same low frequency features around 9 eV in  $U_{dd}$ , while the corresponding feature is absent in both  $U_{pd}$  and  $U_{dd}$ . This indicates that the localized  $p$ - $d$  excitation at 9 eV might be a universal feature of the cuprate compounds.

A useful way to quantify the screening effect is to compute the “renormalization factor”<sup>15</sup>  $Z_B = \exp[\frac{1}{\pi} \int_0^\infty \text{Im } U(\omega)/\omega]$ . In a one-band model, the low-energy properties of the solution for a frequency-dependent interaction  $U(\omega)$  can be reproduced by a cal-

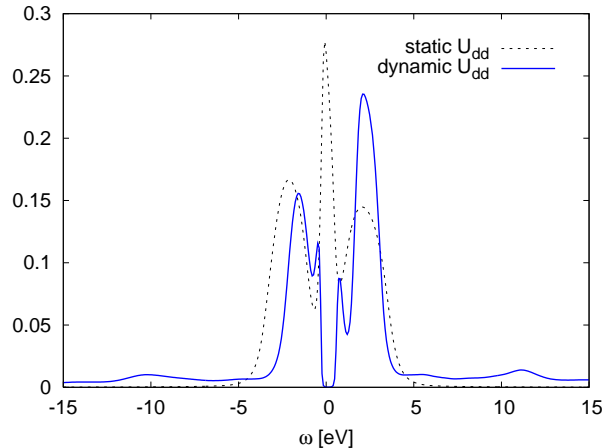


FIG. 3: Local spectral functions for the one-band model with static and dynamic  $U$  (inverse temperature  $\beta = 10$ ). Results obtained via analytical continuation of the self-energy.

culation involving the static interaction  $U(\omega = 0)$  and hopping parameters renormalized by  $Z_B$ . Hence, this factor essentially tells us by how much the static limit underestimates the interaction strength. In the case of  $\text{La}_2\text{CuO}_4$ ,  $Z_B$  is remarkably low. For the one-band model, we find  $Z_B = 0.58$  and for the three-band model  $Z_B^{dd} = 0.52$ . These low values are primarily due to the strong pole near 9 eV. Indeed, for  $U_{pp}$  and  $U_{pd}$  the renormalization factor is higher:  $Z_B^{pp} = 0.68$  and  $Z_B^{pd} = 0.80$ .  $Z_B$  is low for  $\text{La}_2\text{CuO}_4$  even in comparison with other cuprate compounds. For  $\text{HgBa}_2\text{CuO}_4$  for example, where the 9 eV pole is less pronounced, the renormalization factor is  $Z_B = 0.66$  in the one-band model.

#### B. One-band model

We first discuss the results obtained for the one-band model. Figure 3 shows the local  $d$ -electron spectral function obtained with the frequency-dependent interaction (blue line) and with the static interaction  $U_{dd}(0)$  (dashed black curve). The calculations have been performed at temperature  $T = 0.1$  in the paramagnetic phase, and we use the analytical continuation procedure described in Sec. IID. We see that the static interaction is not enough to open a Mott gap in the spectral function, whereas the calculation with the full  $U_{dd}(\omega)$  yields a gap. However, the gap size of  $\lesssim 1$  eV is too small compared to the experimentally measured optical gap of 2 eV.<sup>28</sup> Apart from this low-energy region, the spectra differ mainly at high energies. Here, the dynamic- $U$  spectrum features satellites at energies of approximately  $\pm 9$ -13 eV and a broad plasmon peak centered around 30 eV. They correspond to collective excitations with simultaneous emission or absorption of quantized density fluctuations with a frequency given by the dominant modes visible in Fig. 2. Obviously, this

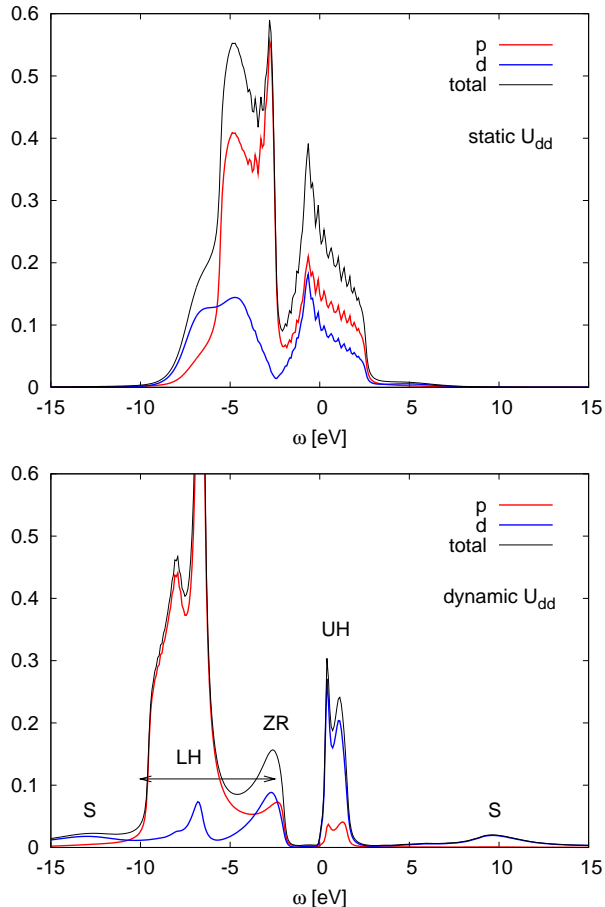


FIG. 4: Local spectral functions for the three-band model with static  $U$  (top panel) and with dynamic  $U$  (bottom panel) at inverse temperature  $\beta = 10$ . We have identified the following features in the  $d$  spectral function: upper Hubbard band (UH), lower Hubbard band (LH), Zhang-Rice singlet band (ZR), and satellites (S). Results obtained via analytical continuation of the self-energy.

physics is missing in a static- $U$  description.

We have also performed a calculation with a static  $U$  but with the one-particle band renormalized by the Bose factor  $Z_B$  as proposed in Ref. 15. This calculation also produces a gap, confirming the importance of the frequency dependence of  $U$  in renormalizing the band width.

### C. Three-band model

In the three-band calculations, we also find that static interactions equal to the static limit of the *ab-initio* estimated interaction parameters are not enough to open a gap in the spectral function (upper panel of Fig. 4). However, as shown in the bottom panel of Fig. 4, if the frequency-dependence of  $U_{dd}$  is considered, an insulating solution is found, with a gap of 1.9 eV. This is in rather

good agreement with the experimentally measured gap. (Our use of the static screened interactions in the Hartree terms implies that this calculation yields a lower bound for the gap size.) Furthermore, since the calculations have been performed in the paramagnetic phase, the gap opening confirms that the insulating nature of  $\text{La}_2\text{CuO}_4$  is of Mott-Hubbard rather than Slater type. We also find, in agreement with Ref. 9, that the interatomic Hartree potential is essential: Without the corresponding shift in the relative  $p$ - $d$  level splitting, the frequency-dependent  $U_{dd}$  would not be enough to open a Mott gap.

In contrast to the one-band result, the  $d$ -spectral function from the three-band calculation is strongly asymmetric, due to the hybridization with the  $p$ -states which lie below the Fermi energy. The states near the lower gap edge have a mixed  $p$ - $d$  character ( $d^8$  ligand hole) and correspond to the “Zhang-Rice” singlet band.<sup>7,31</sup> On the unoccupied side, the  $d$  density of states is peaked near the band edge and extends over an energy range of about 2 eV. This feature may be interpreted as the upper Hubbard band corresponding to the  $d^{10}$  configuration.

While the upper Hubbard band is rather well defined, there have been conflicting results concerning the lower Hubbard band. In view of the discussion in the previous literature about the correct position of the lower Hubbard band<sup>6,7</sup> we have to caution that this feature is difficult to identify due to the dynamical nature of the Coulomb interaction. Especially in  $\text{La}_2\text{CuO}_4$ , which has a prominent screening mode at  $\omega \approx 9$  eV (similar to the screened interaction of  $U_{dd}(\omega = 0) = 7$  eV) structures that may be identified with the lower Hubbard band can be expected to overlap with satellite features. Furthermore, due to the self-consistent adjustment of the  $p$ - $d$  level splitting via the Hartree contribution in Eqs. (4) and (5), which is affected by the smaller  $n_d$  in the dynamic- $U$  calculation, the  $p$ -states are pushed down in energy, so that there is a strong  $p$ - $d$  hybridization in the energy range where we expect the lower Hubbard band.

To shed some light on the satellite issue, we plot in Fig. 5 the  $d$ -electron spectral function for the three-band model. In contrast to Fig. 4, where the density of states has been obtained via the analytical continuation of the self-energy, we computed the spectral function shown in Fig. 5 directly from the local Green’s function, by the procedure explained in Sec. II D. While the direct continuation of the Green’s function yields a somewhat poorer resolution of the features in the energy region dominated by the  $p$ -states, the agreement between the two spectral functions is rather good.

The analytical continuation of  $G$  by the method of Casula *et al.*<sup>29</sup> allows us to identify a “regular” contribution to the density of states, and a “satellite” contribution, corresponding to states which can be accessed via the emission or absorption of bosons. In the regular part, we can identify the upper Hubbard band in the energy region from 0 to 2 eV, the Zhang-Rice singlet band responsible for the peak near the lower gap edge, and a broad feature in the energy range from -3 to -10 eV. It is this latter fea-



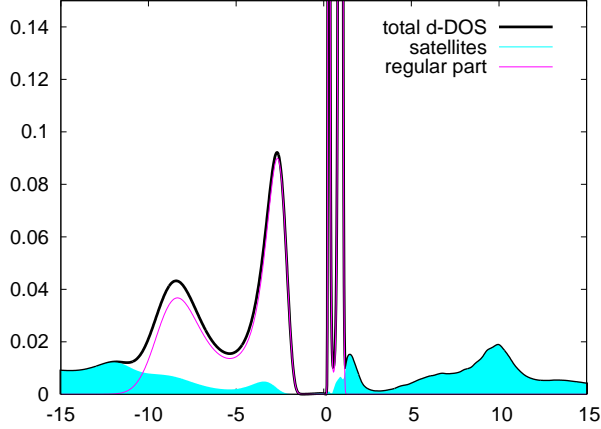


FIG. 5: Local  $d$ -electron spectral function for the 3-band model (inverse temperature  $\beta = 10$ ). Results obtained via analytical continuation of the local Green's function. The black line plots the total spectral function, while the pink line shows  $A_{\text{reg}}(\omega)$  and the blue shaded area the satellite contributions generated by the convolution of  $A_{\text{reg}}(\omega)$  with the bosonic spectral function.

ture which should be associated with the lower Hubbard band. The comparison with Fig. 4 shows that this Hubbard band (which is somewhat more asymmetric in the spectrum based on the analytical continuation of  $\Sigma$ ) overlaps with the  $p$  states, so that the lower Hubbard band is partially masked by  $d$  spectral weight originating from  $p$ - $d$  hybridization. On the other hand, the hump seen in the energy range from -10 to -15 eV, as well as the peak centered around +10 eV, should be considered satellite features which result from the frequency dependence of the Hubbard- $U$  in the effective low-energy model. The position of the satellite feature around -13 eV is in good agreement with the experimental photoemission spectra in Ref. 32.

To reveal the lower Hubbard band, it is instructive to look at the momentum resolved spectral function. In Fig. 6, we plot the  $p$  and  $d$  spectral functions along the same path as in Fig. 1. Besides the weakly dispersing upper Hubbard band we find a similarly dispersing band in the energy range from -2 to -6 eV. The states near the band edge, which have a strong overlap with  $p$  states, may be identified with Zhang-Rice singlets. In the same region of momentum space, one finds an almost dispersionless band at -7 eV, which also exhibits a strong overlap with  $p$  states. This energy is suggestive because it corresponds to the screened  $U_{dd}$ , and the chemical potential is at the upper gap edge. However, a comparison with the LDA bandstructure in Fig. 1 and the  $p$  spectral function shows that this feature in the  $d$  spectral function can be naturally interpreted as originating from the hybridization with a renormalized  $p$  band. Hence, it appears that the  $d$  states which may be associated with the lower Hubbard

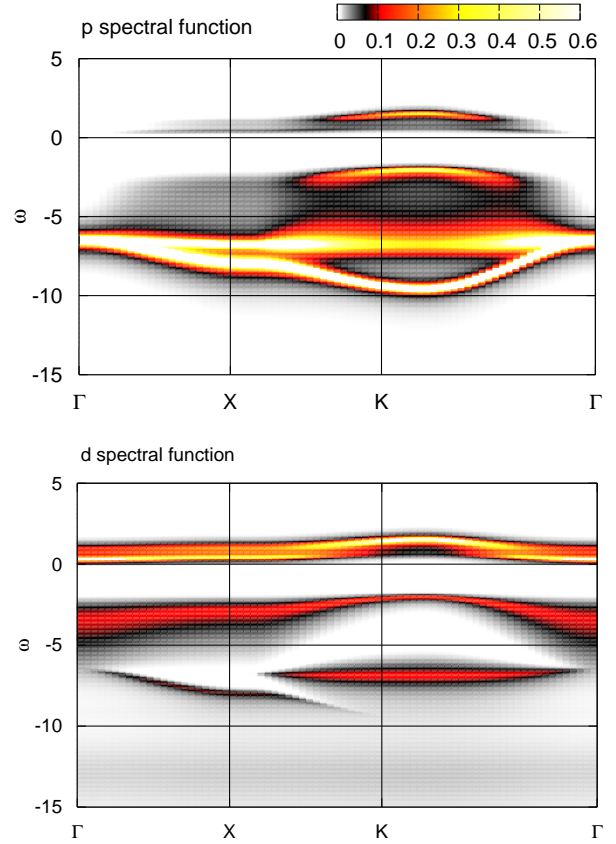


FIG. 6:  $k$ -resolved spectral functions for the three band model at  $\beta = 10$  along the same path as in Fig. 1. Top panel:  $p$ -electron spectral function. Bottom panel:  $d$ -electron spectral function.

band cover a broad energy range up to the gap edge, and that the Zhang-Rice band should be considered a substructure of the lower Hubbard band. Since the lower Hubbard band covers the same energy range as the  $p$  states, and the structure near -13 eV (visible as a grey band in the bottom panel of Fig. 6) is a satellite, our calculation is not consistent with a simple charge-transfer insulator picture, in which the Hubbard band lies below the  $p$ -states.

It is interesting to note that the fully screened interaction  $\text{Im} W_{dd}$  is dominated by two strong peaks at energies 3 and 9 eV which signal the formation of many-body or collective states with those binding energies (Fig. 7). Comparison with  $\text{Im} U_{dd}$  for the one-band or three-band model allows us to conclude that the peak at 3 eV in  $\text{Im} W_{dd}$  originates from collective excitations within the  $d_{x^2-y^2}$  band since the peak is missing in  $\text{Im} U_{dd}$ . This energy happens to be close to the size of the gap. In a weakly correlated system structures in  $\text{Im} W$  must necessarily be carried over to  $\text{Im} \Sigma$  and in turn inherited by the spectral function. Structures in the spectral function must therefore reflect structures in  $\text{Im} W$ . One interest-

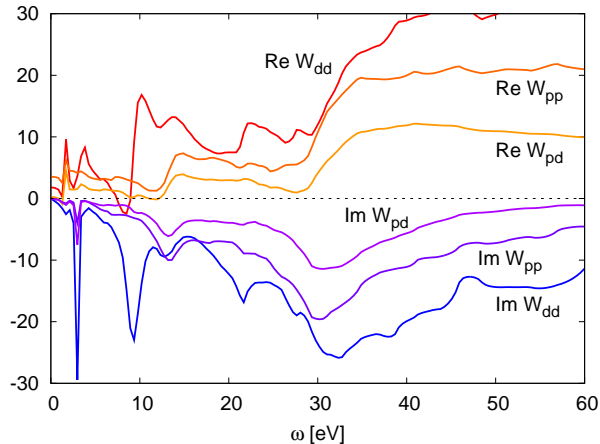


FIG. 7: Fully screened interaction  $W(\omega)$  for the three-band model.

ing but yet unresolved issue is the relation between these peaks in  $\text{Im } W$  and the Hubbard bands.

If the screened interaction  $W$  were computed fully self-consistently, and not by cRPA, transitions across the gap would contribute to the low-energy screening, so that we can expect a feature in  $\text{Im } W_{dd}$  at an energy corresponding to this gap. There is however a priori no reason why the cRPA  $W$ , which is derived from the LDA bandstructure, should exhibit these structures. Whether the agreement between the gap size in Fig. 5 and the sharp peak in  $\text{Im } W$  in Fig. 7 is a mere coincidence, or if the corresponding properties of the bandstructure (used in the DMFT calculation) play a role in fixing the size of the Mott or charge transfer gap is an interesting open question.

#### D. Relationship between one-band and three-band model

We now consider the long-debated question to what extent the one-band model is able to represent the electronic structure of the three-band model and whether the one-band model is sufficient to describe the low-energy physics. The Wannier orbitals in the one-band model are extended objects with both  $p$ - and  $d$ -character. Hence, the lower Hubbard band in this model should not be considered as simply a  $d^8$  state, but rather as a representative of the Zhang-Rice and lower Hubbard bands found in the three-band calculation. Conversely, the upper Hubbard band in the one-band case is not simply a  $d^{10}$  state, but an excitation which has no simple correspondence in the three-band calculation. If we consider the Zhang-Rice singlet band a substructure of the lower Hubbard band, we should compare the separation between the Hubbard bands in the one-band calculation to the separation between upper Hubbard band and the Zhang-Rice band in

the three-orbital model, rather than to the 7 eV gap between the low-energy hump in the lower Hubbard band and the upper Hubbard band. In this case, the agreement between the spectra seems acceptable, given the difference in localization between the Wannier orbitals.

Of course, the one-band calculation cannot reproduce the strong asymmetry of the three-orbital model  $d$ -spectral function, which originates from the presence of the oxygen bands. Also, the gap size is too small, since the calculation does not take into account the effect of  $U_{pd}$ , which is essential in fixing the  $p$ - $d$  level splitting in the three-band calculation.

## IV. SUMMARY

We have constructed low-energy one-band and three-band models for  $\text{La}_2\text{CuO}_4$  from first-principles. The one-particle band structure was based on the LDA and the frequency-dependent effective interaction (dynamic  $U$ ) was calculated using the cRPA method. In both models LDA+DMFT calculations using a static  $U$  taken as the zero frequency limit of the dynamic  $U$  do not yield the expected insulating gap. It is necessary to take into account the frequency-dependent  $U$  in order to open up a gap in the spectrum. This clearly shows the crucial role of dynamical screening in a correct description of the insulating state of  $\text{La}_2\text{CuO}_4$  and in obtaining a consistent picture of the low-energy electronic structure. In agreement with Ref. 9 we have also found that it is important to take into account the change in the inter-atomic Hartree potential, which is neglected in most DMFT calculations, to get the correct position of the oxygen  $p$  band relative to the  $d$  band.

We found that the  $d$  states which should be identified with the lower Hubbard band cover the same energy range as the  $p$  states, and that the Zhang-Rice band should be considered a substructure of the lower Hubbard band. In addition two pronounced collective excitations embodied in the fully screened interaction  $W$  were observed at  $\omega = 3$  and 9 eV. The peak at 3 eV can be traced back to a collective plasmon-like excitation arising from particle-hole excitations within the antibonding  $d$  band whereas the 9 eV peak corresponds to a collective excitation originating from transitions between the occupied oxygen  $p$  bands and the antibonding  $d$  band. The peak at 9 eV is responsible for the very strong screening effect in  $\text{La}_2\text{CuO}_4$ . It also gives rise to satellites in the spectral function at  $-13$  and  $+10$  eV. The peak at  $-13$  eV that may look like the lower Hubbard band is in fact a subplasmon satellite associated with the  $p$ -to- $d$  transitions. The true lower Hubbard band is partially masked by the oxygen  $p$  bands at a lower binding energy.

Comparison between the spectral functions of the one- and three-band models reveals that the one-band model is not sufficient to describe the electronic structure within the energy range of the gap. The size of the gap of the one-band model is significantly smaller than that of the



three-band model, where the latter value of 1.9 eV is in very good agreement with the experimentally measured data of 2.0 eV. It is also quite evident that the one-band model cannot properly describe the true character of the top of the valence band, which is of the type  $d^8$  ligand hole, rather than a simple lower Hubbard band splitting off the antibonding  $d$  band.

While our calculation is based on the *ab-initio* bandstructure, uses *ab-initio* interaction parameters, and takes into account the  $p$ - $d$  interaction (at the Hartree level), one missing ingredient is the momentum-dependence of the self-energy. It has been found in recent studies that the strong band renormalization from the dynamical  $U$  is at least partially compensated by a band-widening due to the  $k$ -dependence of the self-energy.<sup>35–37</sup> Quantifying these effects for  $\text{La}_2\text{CuO}_4$  requires more advanced schemes, such as cluster extensions of DMFT (which cannot be easily combined with the most efficient techniques for treating frequency de-

pendent  $U$ ), or GW+DMFT (which may not properly capture the  $k$ -dependence in strongly correlated compounds<sup>38</sup>). Exploring these issues will be an interesting topic for future studies.

### Acknowledgments

We thank P. Hansmann for helpful discussions. The DMFT simulations have been run on the Brutus cluster at ETH Zurich, using a code based on ALPS.<sup>39</sup> PW has been supported by SNSF grant No. 200021-140648 and NCCR Marvel. Some of this research has been carried out during a stay at ESI (Vienna). This work was also supported by the Swedish Research Council and part of the computations were performed on resources provided by the Swedish National Infrastructure for Computing (SNIC) at LUNARC.

- 
- <sup>1</sup> Y. Kamihara et al., J. Am. Chem. Soc. **130**, 3296 (2008).
  - <sup>2</sup> H. Sakakibara, H. Usui, K. Kuroki, R. Arita, and H. Aoki, Phys. Rev. Lett. **105**, 057003 (2010).
  - <sup>3</sup> H. Sakakibara, H. Usui, K. Kuroki, R. Arita, and H. Aoki, Phys. Rev. B, **85**, 064501 (2012).
  - <sup>4</sup> O. K. Andersen, A. I. Lichtenstein, O. Jepsen, and F. Paulsen, Journal of Physics and Chemistry of Solids **56**, 1573 (1995).
  - <sup>5</sup> V. J. Emery, Phys. Rev. Lett. **58**, 2794 (1987).
  - <sup>6</sup> C. Weber, K. Haule and G. Kotliar, Phys. Rev. B **78**, 134519 (2008).
  - <sup>7</sup> L. de Medici, X. Wang, M. Capone, and A. J. Millis, Phys. Rev. B **80**, 054501 (2009).
  - <sup>8</sup> H. Das and T. Saha-Dasgupta Phys. Rev. B **79**, 134522 (2009).
  - <sup>9</sup> P. Hansmann, N. Parragh, A. Toschi, G. Sangiovanni, K. Held, New Journal of Physics **16**, 033009 (2014).
  - <sup>10</sup> A. Damascelli, Z. Hussain, and Z-X. Shen, Rev. Mod. Phys. **75**, 473 (2003).
  - <sup>11</sup> F. Aryasetiawan, M. Imada, A. Georges, G. Kotliar, S. Biermann, and A. I. Lichtenstein, Phys. Rev. B **70**, 195104 (2004).
  - <sup>12</sup> P. Werner, A. J. Millis, Phys. Rev. Lett. **104**, 146401 (2010).
  - <sup>13</sup> P. Werner, M. Casula, T. Miyake, F. Aryasetiawan, A. J. Millis, S. Biermann, Nature Phys. **8**, 331 (2012).
  - <sup>14</sup> L. Huang and Y. Wang, Europhys. Lett. **99**, 67003 (2012).
  - <sup>15</sup> M. Casula, Ph. Werner, L. Vaugier, F. Aryasetiawan, T. Miyake, A. J. Millis, and S. Biermann Phys. Rev. Lett. **109**, 126408 (2013).
  - <sup>16</sup> B. P. P. Mallett, T. Wolf, E. Gilioli, F. Licci, G. V. M. Williams, A. B. Kaiser, N. W. Ashcroft, N. Suresh, and J. L. Tallon, Phys. Rev. Lett. **111**, 237001 (2013).
  - <sup>17</sup> www.flapw.de.
  - <sup>18</sup> N. Marzari and D. Vanderbilt, Phys. Rev. B **56**, 12847 (1997).
  - <sup>19</sup> I. Souza, N. Marzari and D. Vanderbilt, Phys. Rev. B **65**, 035109 (2001).
  - <sup>20</sup> A. Mostofi, J. R. Yates, Y.-S. Lee, I. Souza, D. Vanderbilt, and N. Marzari, Comput. Phys. Commun. **178**, 685 (2008).
  - <sup>21</sup> F. Freimuth, Y. Mokrousov, D. Wortmann, S. Heinze, and S. Blügel, Phys. Rev. B **78**, 035120 (2008).
  - <sup>22</sup> R. Sakuma, Phys. Rev. B **87**, 235109 (2013).
  - <sup>23</sup> A. Georges, G. Kotliar, W. Krauth, and M. J. Rozenberg, Rev. Mod. Phys. **68**, 13 (1996).
  - <sup>24</sup> P. Werner, A. Comanac, L. De Medici, M. Troyer, A. J. Millis, Phys. Rev. Lett. **97**, 076405 (2006).
  - <sup>25</sup> P. Werner and A. J. Millis, Phys. Rev. Lett. **99**, 146404 (2007).
  - <sup>26</sup> V. I. Anisimov, J. Zaanen, and O. K. Andersen, Phys. Rev. B **44**, 943 (1991).
  - <sup>27</sup> Use of the LDA density in the double counting term for the  $d$  band would push the  $d$  bands down into the  $p$  bands and result in a metallic solution. This is because  $n_d^{\text{LDA}} \approx 1.5$  is considerably higher than the  $n_d \approx 1.1$  of the insulating solution.
  - <sup>28</sup> J. M. Ginder, R. M. Roe, Y. Song, R. P. McCall, J. R. Gaines, E. Ehrenfreund, and E. J. Epstein, Phys. Rev. B **37**, 7506 (1988).
  - <sup>29</sup> M. Casula, A. Rubtsov, and S. Biermann, Phys. Rev. B **85**, 035115 (2012).
  - <sup>30</sup> M. Jarrell and J. E. Gubernatis, Phys. Rept. **269**, 133 (1996).
  - <sup>31</sup> F. C. Zhang and T. M. Rice, Phys. Rev. B **37**, 3759 (1988).
  - <sup>32</sup> Z.-X. Shen, *et al.*, Phys. Rev. B **36**, 8414 (1987).
  - <sup>33</sup> M. Gatti and M. Guzzo, Phys. Rev. B **87**, 155147 (2013).
  - <sup>34</sup> M. Gatti, F. Bruneval, V. Olevano, and L. Reining, Phys. Rev. Lett. **77**, 266402 (2007).
  - <sup>35</sup> T. Miyake, C. Martins, R. Sakuma, and F. Aryasetiawan, Phys. Rev. B **87**, 115110 (2013).
  - <sup>36</sup> R. Sakuma, P. Werner, F. Aryasetiawan, Phys. Rev. B **88**, 235110 (2013).
  - <sup>37</sup> A. van Roekeghem *et al.*, arXiv:1408.3136.
  - <sup>38</sup> T. Ayral, S. Biermann and P. Werner, Phys. Rev. B **87**, 125149 (2013).
  - <sup>39</sup> A. Albuquerque *et al.*, Journal of Magnetism and Magnetic Materials **310**, 1187 (2007).